Optimization of resonant dielectric multilayer for enhanced fluorescence imaging

A Mouttou, F Lemarchand, C Koc, A Moreau, J Lumeau, C Favard, Aude L. L. Lereu

Optical Materials: X 17 (2023) 100223

Contents lists available at ScienceDirect

Optical Materials: X

journal homepage: www.elsevier.com/locate/omx

Invited article

Optimization of resonant dielectric multilayer for enhanced fluorescence imaging

A. Mouttou [a,b], F. Lemarchand [b], C. Koc [b], A. Moreau [b], J. Lumeau [b], C. Favard [a,*], A.L. Lereu [b,*]

[a] Institut de Recherche en Infectiologie de Montpellier, CNRS, Univ of Montpellier, Montpellier, France
[b] Aix Marseille Univ, CNRS, Centrale Marseille, Institut Fresnel, Marseille, France

ARTICLE INFO

Keywords:
Optical thin film
Evanescent field
Fluorescence imaging

ABSTRACT

In the aim of improving the sensitivity in objective-based total internal reflection fluorescence microscopy (ob-TIRF-M), we recently investigated the use of resonant dielectric multilayer (DM) coated coverslips while considering the experimental constraints of commercial ob-TIRF-M. The imaginary part of the refractive index k of the DM top layer material was then shown to be a key parameter to control during the DM optimization in order to limit the discrepancies between theory and experiment. We therefore report here on the development, fabrication and implementation of a specific top layer with a controlled k. This latter was first investigated as a single layer to accurately define its optical properties while adjusting the stoichiometric conditions during deposition. The DM optimization method was then fully revised to include its optical parameters. By doing so, the optimization was freed from the strong dependence on k and we observed a good agreement between the expected and measured fluorescence signal enhancement. This was illustrated by numerically calculating the fluorescence signal enhancement as a function of the top layer k and by comparing it to fluorescent beads imaging over three DM of different k.

1. Introduction

In total internal reflection fluorescence microscopy (TIRF-M), the use of evanescent waves makes it possible to observe events occurring at the interface between the microscope coverslip and the biological sample [1,2]. In the cell, this is the plasma membrane, where many processes take place such as endo/exocytosis or cell adhesion which are fundamental for cell survival. It is also at the plasma membrane that many human pathogenic viruses (HIV, Sars-CoV2, Influenza) assemble and bud. TIRF-M is therefore widely used as an observation method in many fields of membrane biology. If this technique is relatively simple to use, its sensitivity as well as its lateral resolution remain limiting factors for the study of nanometer-sized objects such as viruses. For the lateral resolution limitation, TIRF-M has been coupled to single molecule localization as in PALM (PhotoActivation Localization Microscopy) [3], STORM (STochastic Optical Reconstruction Microscopy) [4]. More recently, TIRF-M was indeed combined with super-critical angle fluorescence detection for high axial resolution and sharp localization pointing precision [5]. In the field of virology, these techniques have proven their strength and use [6–11]. For the lack of sensitivity, as the fluorescence emission is, among others, proportional to the intensity of the excitation field, we proposed to act on the local evanescent exciting field by introducing resonant dielectric multilayer (DM) coated coverslips while limiting its impact over the fluorescence collection efficiency. Similar to surface plasmon-based (SPs) microscopy techniques [12–15], Bloch-surface waves (BSWs), supported by resonant DM, can be used in fluorescence microscopy to enhance the fluorescence signal [16–25]. Moreover, despite the opto-geometric similarities between SPs and BSWs [26–29], BSWs bring new insights in the context of fluorescence imaging, as they can be designed with no limitation over the illumination conditions and they are bio-compatible with a low quenching impact over the fluorophores.

Starting from the admittance formalism in optical thin solid films, we classically developed resonant DM for sensing applications with sharp and intense resonances [30–34] resulting in maximum field enhancement factors of 10^3 - 10^4 associated with an angular resonance tolerance of few μrad. However, these resonances are also highly depending on the illumination bandwidths [35] and on the fabrication tolerances [36]. In fluorescence imaging, the desired resonances require a fully-rethought design with different optical performances: 1- a field enhancement of few tenths is enough to prevent photobleaching and 2- an angular tolerance of the resonance in the order of the illumination divergence, classically above 10 mrad in classical objective-based TIRF-M. This was reported in [25]. Following our recent study, we describe here the optimization method to design a DM with the best electric

* Corresponding authors.
E-mail addresses: cyril.favard@irim.cnrs.fr (C. Favard), aude.lereu@fresnel.fr (A.L. Lereu).

https://doi.org/10.1016/j.omx.2022.100223
Received 13 October 2022; Received in revised form 5 December 2022; Accepted 7 December 2022
Available online 9 December 2022

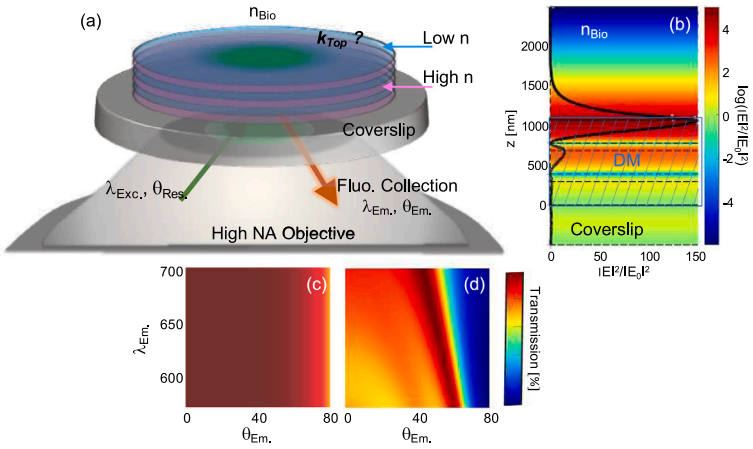

Fig. 1. (a) Experimental set up of the objective-based e-TIRF-M with a dielectric multilayer design optimized for a TE-polarized excitation at $\lambda_{Exc.}$ = 561 nm, $\theta_{Res.}$ = 68°. The fluorescence is then collected through the objective over a spectral and angular range $\lambda_{Em.}$, $\theta_{Em.}$. (b) Predicted field distribution through the stack under plane wave conditions, with a large evanescent field at the interface with the biological environment of refractive index n_{Bio}. (c) and (d) Transmission response over the fluorescence spectral and angular range for a classical glass coverslip and a coated one, respectively. The average transmission of the proposed DM-coated coverslip is estimated at 58% against 96% for a glass coverslip.

field enhancement and to be adapted to microscopy constraints. We then investigated the effect of the imaginary part of the refractive index k of the top layer of the DM in direct contact with the biological environment over the fluorescence enhancement. To experimentally demonstrate the concept, we established a protocol to fabricate such specific single layer with a controlled k by acting on its stoichiometry during deposition. We showed that, by using the reported optimization method, for $k < 10^{-4}$ (classically the case in dielectric thin films), this key parameter k is no longer influencing and impacting the fluorescence enhancement. We finally tested this new concept on fluorescent beads, using three DM structures of various stoichiometry for the top layer, a good agreement with the predicted fluorescence enhancement was observed.

2. Enhanced-TIRF-M configuration

The enhanced-TIRF-M (e-TIRF-M) concept is described in (Fig. 1a), where the DM coated coverslip is a typical glass coverslip coated with an alternation of thin layers of high and low indices dielectric materials. The top layer is chosen to be made of SiO_i with $i \leq 2$ to ensure the biocompatibility and to secure cell adhesion. In addition, the total thickness of the DM is kept in the order of 1 to 2 μm to remain compatible with the high numerical aperture corrected objectives and avoid introducing optical aberrations. (Fig. 1b) represents the electric field distribution through the DM coated coverslip under TE-polarized plane wave illumination using an excitation wavelength $\lambda_{Exc.}$ = 561 nm and an incidence of $\theta_{Res.}$ = 68°. The hatched area highlights the DM surrounded by the glass coverslip on one side and the biological environment (n_{Bio}) on the other side. The black lines in Fig. 1b represent the calculated field distribution along the z-axis. It is to be noted that by tuning the field enhancement at an angle $\theta_{Res.}$ = 68°, the penetration depth d ($|E(z=d)|^2 = e^{-1}.|E(z=0)|^2$) decreases from 540 nm at the classical TIRF angle (θ = 63°) on a glass coverslip to 110 nm in our e-TIRF-M.

The fluorescence experiment is carried out using an objective-based TIRF-microscope (Nikon Eclipse Ti) with an illumination through a 1.49 NA objective using a 25 μW laser line of wavelength $\lambda_{Exc.}$ and TE-polarized, in accordance to the resonance optimization conditions ((Fig. 1a)). Thanks to the high NA objective, the incident angle, at the interface with the biological environment, can be scanned from 0 to 81°. In addition, the collection of the fluorescence is managed through the same objective over a large spectral and angular emission range ($\lambda_{Em.} \in$ [550-–700 nm], $\theta_{Em.} \in$ [0 - 80°]). With such configuration, the DM can impact the fluorescence collection efficiency so one has to take into account the DM transmission over the fluorescence collection with respect to a glass coverslip. Figs. 1(c) and (d) give the calculated transmissions over the emission range for a glass coverslip (c) and a DM-coated coverslip (d). After filtering steps through a 575 nm long-pass dichroic and a 579 nm long-pass emission filter, the fluorescence emission is recorded using an EM-CCD camera (Evolve 512) with a time exposure set at 200 ms. Finally, as we reported in [25], the angular beam divergence has a strong impact over the fluorescence enhancement, therefore, prior to each measurement the divergence is experimentally measured with a precision below 1 mrad. However, even when taking into account the incident beam angular divergence and the collection efficiency, the predicted fluorescence enhancement is always higher than the measured one. We thus revisited the design of the DM structure to terminate them by a top single layer with controlled k.

3. Optimization of dielectric multilayer with controlled absorption

In previous work [30–34], we reported on an analytical technique for synthesizing dielectric multilayers delivering the optimum optical field enhancement in response to an arbitrary excitation. This technique uses the admittance formalism, under total internal reflection condition, by either optimizing the absorption to be total (A=100%) [30–32], or canceling the complex admittance [33,34], at the free interface. With this analytical synthesis, we can adapt resonant DM regardless the layers materials and the illumination parameters (i.e. wavelength, incidence and polarization) to support sharp and intense optical resonances associated to a field enhancement. This latter is directly linked to the inverse of the imaginary index of the DM top layer. These resonances have great advantages for sensing applications but have to be rethought for the TIRF-M applications, where the design of the DM has to consider different parameters:

1. The field enhancement has to be maximized at the interface with the biological medium, under a fixed wavelength, at a given angle.
2. The enhancement factor must be in the order of tens to hundreds to be suitable for e-TIRF-M i.e. improving the signal to noise ratio without generating strong fluorophore photobleaching.
3. The field value must be integrated over a solid angle cone typically in the order of 1° in accordance with the incident divergence that is between 0.2 and 1.5° in commercial TIRF-M,

i.e. the angular tolerance of the resonance must be optimized accordingly. The angular dependency of the electric field for a divergent beam was then introduced as $\xi_{\Delta\theta}(\theta)$ as described in [25].

4. The DM average transmission T_{av} must be maximized between 0 and 81° and from 570 to 700 nm (for $\lambda_{Exc.}$ = 561 nm) to achieve the best fluorescence collection signal.

Therefore, to optimize this dedicated structure, we started from a typical resonant structure [30–33] consisting of alternating quarter-waves of high (H) and low (L) refractive index materials at the desired wavelength and incidence, and terminating with a top layer of L-type, here SiO_2, of thickness t (i.e. Bio / $tL-(HL)^3$ / Glass). The synthesis is done to optimize the field value at the free interface. From our previous work [25], we assigned the discrepancies between predicted and experimental fluorescence signals to the lack of control over the key parameter that is the imaginary part of the top layer k. This k parameter is classically fixed at 10^{-5} for dielectric thin films. Indeed, all spectroscopic methods, including spectrophotometry or ellipsometry have limited sensitivity that do not allow measuring accurately extinction coefficients down to the 10^{-5}–10^{-6} range. Unlike the real part of the refractive indices, the imaginary part values can be extracted from these measurements but with very large uncertainties that are not compatible with our applications. For example, we numerically showed that by only shifting k from 10^{-5} to 2.10^{-5}, the predicted fluorescence enhancement goes from ×5 down to no enhancement with respect to a glass coverslip [25]. This was also experimentally observed, and confirmed the need to control the top layer k value.

To take into account k in the optimization, we modified the classical structure Bio / $tL-(HL)^3$ / Glass to Bio / $t'L'-(HL)^3$ / Glass with t' the new thickness of the top layer and L' its material where L'=SiO_i with $i \leq 2$. The t' must be thick enough to avoid fabrication inhomogeneities but was also imposed to be $\leq$ 30 nm thick, to limit the total absorption of SiO_i that would decrease the resulting field enhancement. By changing the top layer material, we modified the DM operating point defined by the excitation wavelength and incident angle. In order to retrieve the proper operating point, imposed by the biological application, we adjusted t' as well as the thicknesses of the $(HL)^3$ that are no longer quarter-waves.

Within this optimization method, we also considered the transmission response of the DM structure, by maximizing the transmission over the emission spectral and angular range. In the presented structure we achieved a calculated average transmission efficiency of 58% for emission angles from 0 to 60° (Fig. 1d). Although lower than glass transmission efficiency, the gain in sensitivity is preserved thanks to the 10 to 20 times enhancement of the excitation field. Finally, we numerically evaluated the effect of a variation of the k value of the SiO_i layer on the fluorescence signal, for example, a 10^{-3} variation in the k value is predicted to modify the fluorescence signal by only 0.5%. We will discuss thereafter that, using the proposed optimization, the k value has no longer the same drastic impact over the optical response of the DM.

4. Realization of SiO_x with controlled absorption

To implement the concept, we first numerically evaluated the influence of tuning the oxygen level over the k value of a single layer in (Fig. 2a). To do so, we first considered a layer of SiO_2 with a value of k increasing during the deposition to simulate the change in oxygen level. Initially, the predicted transmission T, equal to 86.40%, corresponds to the transmission of a bare high refractive glass such as LAH66 of refractive index n=1.74. Classically, during deposition of transparent material with a lower index than the substrate, the transmission is expected to first go through a maximum (about 91.3% for silica) before returning exactly to the initial value (86.40%). The resulting optical thickness of the simulated first single layer is then equal to $\lambda/2$ for the

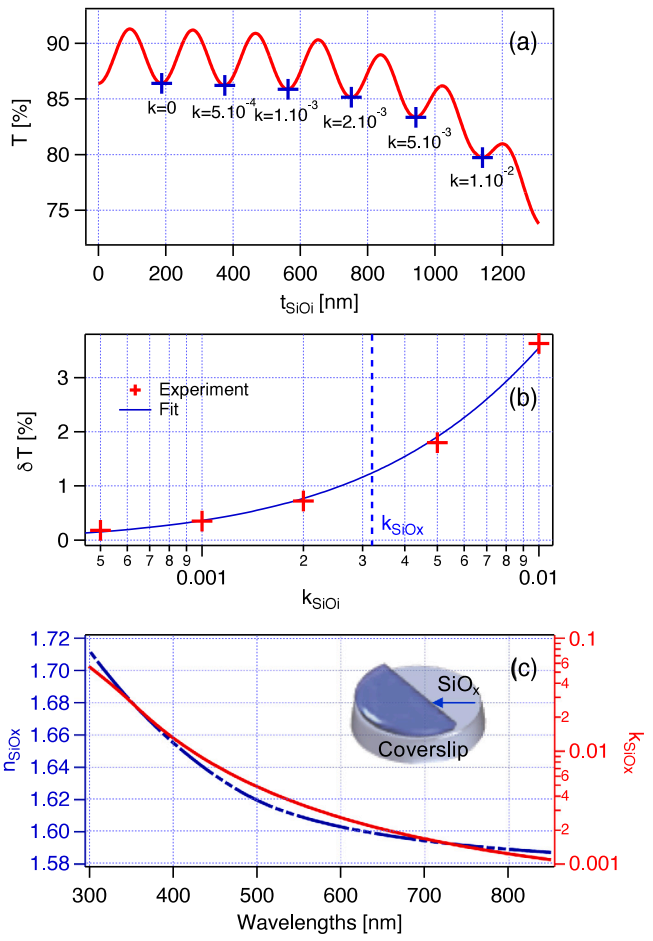

Fig. 2. (a) Calculated transmission as a function of k values to simulate the oxygen level during deposition of SiO_i with $i < 2$. Following the transmission during the deposition of successive $\lambda/2$ single layers of SiO_i for different i, we can predict the resulting k value associated to the transmission (a,b). This allows determining the deposition parameters to make a SiO_x single layer with a k of $3.2.10^{-3}$ at 561 nm (blue dashed line in b). A single layer was then deposited to precisely determine its complex refractive index $\tilde{n}$ as a function of wavelengths by spectrophotometry (c) with $\tilde{n}$(561 nm)=1.602+i3.2.10^{-3}.

considered wavelength (here 561 nm) with a corresponding physical thickness of 187 nm. During the deposition of the next 187 nm single layer, associated to a different oxygen level, the complex refractive index of the deposited layer is assumed to be equal to (n =1.5, k= 5.10^{-4}). The predicted transmission is no longer expected to be equal to 86.40%, but to 86.22%. The associated δT = 0.18% ((Fig. 2b)) lost corresponds to the absorption of the second half-wave layer. A third half-wave layer is then assumed with a k = 1.10^{-3}, and the associated transmission is expected to be T=85.87%, or a δT = 0.35%, signature of the value of k. This process is reiterated for values of k up to 10^{-2}. We have thus established a correspondence between the k value and the transmission drop occurring between two successive depositions of half-wave single layers of SiO_i, see Figs. 2(a) and (b).

To experimentally reproduce this, Plasma Assisted Reactive magnetron sputtering (PARMS) using a Bühler Leybold Optics HELIOS machine was implemented. Sputtering was carried out using a pure Si target and SiO_i material was then obtained by tuning the oxygen level at the plasma assistance level by steps during deposition to reach the predicted T values associated to the desired k values. We thus obtained a k=$3.2.10^{-3}$ for an oxygen level of 5.7 sccm for the L'=SiO_x layer. Note that to classically obtain SiO_2, we have to introduce 50 sccm of oxygen . A single layer of SiO_x was then characterized by spectrophotometry to precisely extract the complex refractive index as a function

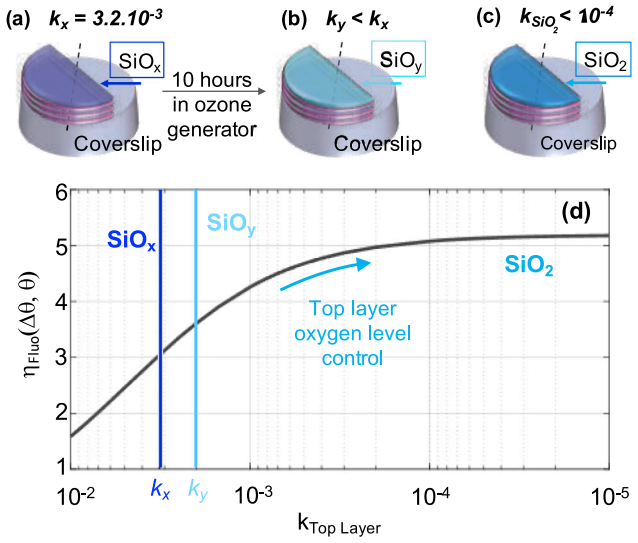

Fig. 3. (a) and (b) Dielectric multilayer structures manufactured by Plasma Assisted Reactive Magnetrons Sputtering with the top layer of different k_i. (b) is the same DM structure as (a) but subjected to an oxygen plasma for 10 h, in order to increase the oxygen level of its top layer and therefore decreasing the k from k_x to k_y. (c) represents the same DM design but with a top layer of SiO_2 and the H material=Nb_2O_5. This structure was manufactured by Plasma Assisted Ion Beam Deposition. (d) Predicted fluorescence enhancement η_{Fluo} structure as a function of the extinction coefficient $k_i \in [10^{-5} - 10^{-2}]$ of the last SiO_i single layer. This is obtained for the resonance conditions $\lambda = 561$ nm, $\theta = 68°$, and for a classical divergence in TIRF-M of $\Delta\theta = 10$ mrad. We observe that a plateau in terms of fluorescence enhancement is reached with this structure for k lower than 10^{-4}.

of wavelengths in Fig. 2(c), with $\tilde{n}(561\ nm)=1.602+i3.2.10^{-3}$. This refractive index of the SiO_x single layer was then used to fine-tune the optimization and to fabricate the dedicated structure described above.

5. Impact of k variations of the top layer over the fluorescence enhancement

In order to evaluate the robustness of the proposed optimization with respect to the k parameter, we numerically estimated the fluorescence enhancement factor η_{Fluo} for different k values for the top layer, ranging from 10^{-5} to 10^{-2}, while keeping the same physical thickness t' as illustrated in Fig. 3(d). For k values smaller than k_{SiOx}, we observed an increase in the fluorescence enhancement which reaches a plateau toward an enhancement factor of 5 for a considered angular divergence of 10 mrad. This assumed that by replacing the SiO_x top layer by a SiO_2 layer of the same physical thickness, the optimized DM structure should enhance the fluorescence even more.

To experimentally confirm the k impact over the fluorescence enhancement, we first fabricated and implemented the proposed DM_{SiOx}, Fig. 3(a). This sample was then subjected to ozone treatment for 10 h to modify its stoichiometry. By increasing the oxygen level, we expect to decrease the k value of the top layer from SiO_x to SiO_y with $y > x$ (Fig. 3(b)), and consequently increase the fluorescence enhancement. For both cases, the used materials, below the top layer, are HfO_2 for the high index material H and SiO_2 for the low index material L. Finally, we pushed further the concept to prove the stability and robustness regarding the deposited materials as well as the deposition technique. For that a third sample, denoted DM_{SiO_2} (Fig. 3(c)) as the top layer is made of SiO_2, was made using plasma assisted ion beam deposition instead of PARMS, and the deposited H-material was changed from HfO_2 to Nb_2O_5. We only adapted the physical thicknesses of each layer according to their refractive indices n and to the optical thicknesses extracted from the initially optimized DM_{SiOx} structure (with HfO_2, SiO_2). Note that from the predicted curve of the fluorescence enhancement as a function of k (Fig. 3(d)), we could design the DM_{SiO_2} structure without specifying the k value of top layer as long as $k < 10^{-4}$. This is another strong advantage of the proposed optimization.

For the three considered DM coated coverslips, we numerically evaluated the field distribution when illuminated by plane waves at the resonance conditions. We evidenced the expected large field, at the interface with the biological medium, that increases as the k value decreases (i.e. from SiO_x to SiO_2) as shown in Fig. 4(a). Furthermore, to predict the resonance conditions, we kept the fixed excitation wavelength at 561 nm and calculated the electric field at the free interface as a function of the incident angles. We thus estimated the resonance angle for each DM at 68° for DM_{SiOx} (used during optimization), at 67.9° for DM_{SiOy} and 69.3° for DM_{SiO_2}, see Fig. 4(b). This angular shift is associated to the variation of the real part of the refractive index n of the top layer occurring when acting on the top layer oxygen stoichiometry. Indeed, when modifying the top layer stoichiometry to change the k value, we also act on its n value. We also confirmed that when the field enhancement increases, the full width at half maximum (FWHM) of the resonance decreases from 0.16° for DM_{SiOx}, to 0.13° for DM_{SiOy} and even 0.038° for DM_{SiO_2}. This effect impacts then the angular tolerance of the DM. Therefore, for the fluorescence enhancement in an objective-based TIRF microscope, one has to compromise between large field enhancement and angular tolerance. We then calculated the expected fluorescence signal as a function of incident angles and extracted the maxima with respect to a glass coverslip. The maxima were obtained at the predicted angular positions mentioned above, as seen in Fig. 5(a). In addition, the fluorescence signal is expected to be ×2.91, ×3.45 and ×4.86 with respect to the glass coverslip, for DM_{SiOx}, DM_{SiOy} and DM_{SiO_2} respectively.

To confirm the predicted optical responses for each fabricated DM, fluorescence measurements were then performed as a function of incident angles using objective-based TIRF microscopy and obtained values were compared to the glass coverslip case. The measurements, shown in Fig. 5(b), were done using 200 nm diameter fluorescent beads excited with a 561 nm incident beam with a divergence of 10 mrad. The recorded fluorescence images, insets Fig. 5(b), were acquired at each defined resonance angles and showed fluorescence signals much higher than on classical glass coverslip for the three cases. The measured fluorescence enhancements (Fig. 5(b)) on the three structures are in very good agreement with the predicted ones (Fig. 5(a)), showing the clear importance of considering the k value when using admittance-based optimizations. This also shows the real strength of the proposed optimization where the top layer k value is no longer a limitation for $k < 10^{-4}$, which is mainly the case for dielectric thin film layers.

6. Conclusion

With the proposed structures containing an absorbing layer with a precisely measured extinction coefficient, we have obtained experimental results of fluorescence measurements in objective-based e-TIRF-M that are in a very good agreement with the theoretical calculations. For that, after taking into account both the large beam divergence of the excitation over the DM resonance as well as optimizing the transmission efficiency of the DM over the fluorescence collection range, we thoroughly investigated numerically and experimentally the impact of the top layer imaginary part of the refractive index k. We confirmed the importance of this parameter when using admittance-based optimization. However, by investigating this impact, we actually established an optimization method no longer absorption-based and therefore independent of k. Indeed, we observed that for $k < 10^{-4}$, the fluorescence enhancement reached a plateau underlying the invariance in k. We observed that a variation around the top layer k will not drastically affect the resulting excitation field, highlighting the stability of the proposed DM structures optimization with respect to the k value. Finally, we have also shown the stability of our concept with respect to the deposited materials and the used deposition technique. This opens new avenues for a simple and widespread production and use of the DM coated coverslip for TIRF-M.

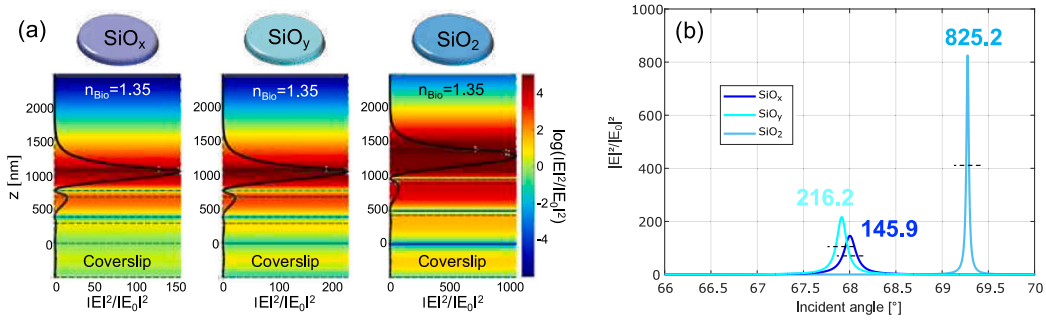

Fig. 4. (a) Electric field distribution within the DM along the azimuth z for the three considered k values. This is obtained under plane wave illumination for the resonance conditions ($\lambda_{Exc.}$ = 561 nm). (b) Electric field enhancement at the interface with the biological medium as a function of incident angles. At the free interface, we clearly evidenced the field enhancement that increases as k decreases (a) and (b). In (b), we also evaluated the angular shift associated to the variation of n occurring when changing the stoichiometry of the top layer. We also showed that when the enhancement increases the full width at half maximum of the resonance decreases. This is a compromise in the e-TIRF-M that limits in overall the fluorescence enhancement.

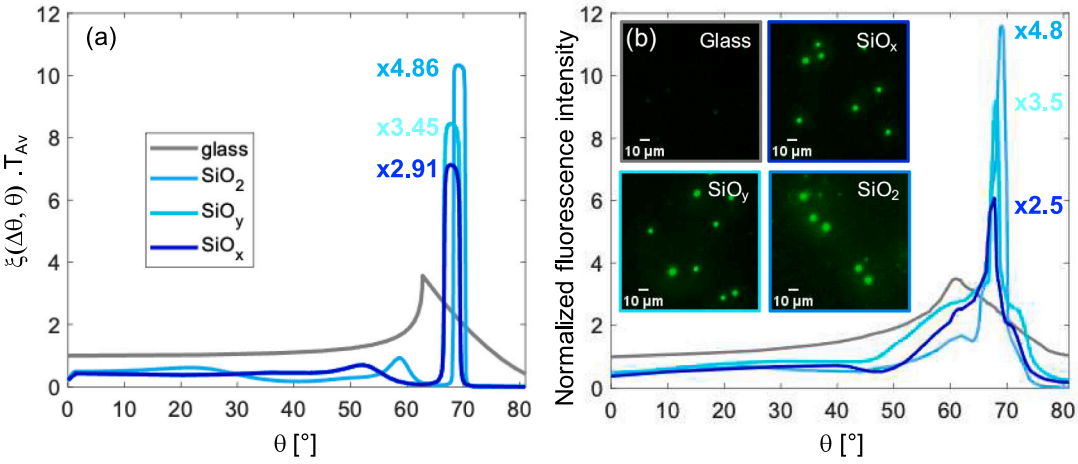

Fig. 5. (a) Theoretical calculation of the angular distribution of the fluorescence intensity, defined by $\xi_{\Delta\theta}(\theta).T_{Av}$, for the three samples (blue curves) compared to classical glass coverslip (gray curve) for a divergence in objective-based TIRF-M of $\Delta\theta$ = 10 mrad. This evidences the impact of k_i over the fluorescence signal. (b) Experimental measurements of beads fluorescence intensity performed on SiO_x, SiO_y and SiO_2 DM structures. The inset gives the associated fluorescence images for each case under resonance conditions. This shows the good agreement with the predicted fluorescence signal but also with the expected angular position shift of the resonance from one structure to another.

CRediT authorship contribution statement

A. Mouttou: Interpreted the results, Wrote & approved the manuscript, Made the thin film sample, Performed the fluorescence experiments. **F. Lemarchand:** Led the optimization developments, Interpreted the results, Wrote & approved the manuscript. **C. Koc:** Made the thin film samples, Interpreted the results, Wrote & approved the manuscript. **A. Moreau:** Made the thin film samples, Performed the fluorescence experiments, Interpreted the results, Wrote & approved the manuscript. **J. Lumeau:** Proposed & designed the study, Interpreted the results, Wrote & approved the manuscript. **C. Favard:** Proposed & designed the study, Interpreted the results, Wrote & approved the manuscript. **A.L. Lereu:** Proposed & designed the study, Interpreted the results, Wrote & approved the manuscript.

Declaration of competing interest

The authors declare that they have no known competing financial interests or personal relationships that could have appeared to influence the work reported in this paper.

Data availability

Data will be made available on request.

Acknowledgments

This work was sponsored by the CNRS through the MITI - Mission for Transversal and Interdisciplinary Initiatives 2017 and the AAP 80|PRIME 2019. This work was also supported by the French National Research Agency through the AAPG 2020 - ANR NIS. The authors acknowledge Dr D. Muriaux for fruitful discussions and the Centre d'Etudes des Maladies Infectieuses et Pharmacologie Anti-Infectieuse (CEMIPAI) and Montpellier Ressources Imagerie (MRI) facilities for access to the commercial TIRF-M. The authors thank Olivier Hector for his help during deposition of the dielectric structures.

C. Favard is a member of the CNRS consortium GDR Imabio.

References

[1] D. Axelrod, N.L. Thompson, T.P. Burghardt, J. Microsc. (ISSN: 0022-2720) 129 (1983) 19–28.
[2] M. Oheim, Lasers Med. Sci. (ISSN: 0268-8921) 16 (2001) 159–170.
[3] E. Betzig, G.H. Patterson, R. Sougrat, O.W. Lindwasser, S. Olenych, J.S. Bonifacino, M.W. Davidson, J. Lippincott-Schwartz, H.F. Hess, Science (ISSN: 1095-9203) 313 (2006) 1642–1645.
[4] M.J. Rust, M. Bates, X. Zhuang, Nature Methods (ISSN: 1548-7091) 3 (2006) 793–795.
[5] N. Bourg, C. Mayet, G. Dupuis, T. Barroca, P. Bon, S. Lécart, E. Fort, S. Lévêque-Fort, Nat. Photonics (ISSN: 1749-4893) 9 (9) (2015) 587–593.
[6] K. Inamdar, C. Floderer, C. Favard, D. Muriaux, Viruses (ISSN: 1999-4915) 11 (2019).

[7] K. Inamdar, F.-C. Tsai, R. Dibsy, A. de Poret, J. Manzi, P. Merida, R. Muller, P. Lappalainen, P. Roingeard, J. Mak, P. Bassereau, C. Favard, D. Muriaux, ELife (ISSN: 2050-084X) 10 (2021).
[8] C. Floderer, J.-B. Masson, E. Boilley, S. Georgeault, P. Merida, M. El Beheiry, M. Dahan, P. Roingeard, J.-B. Sibarita, C. Favard, D. Muriaux, Sci. Rep. (ISSN: 2045-2322) 8 (2018) 16283.
[9] G.W. Ashdown, G.L. Burn, D.J. Williamson, E. Pandzić, R. Peters, M. Holden, H. Ewers, L. Shao, P.W. Wiseman, D.M. Owen, Biophys. J. (ISSN: 1542-0086) 112 (2017) 1703–1713.
[10] C.V. Carman, Methods Mol. Biol. (Clifton, N.J.) (ISSN: 1940-6029) 757 (2012) 159–189.
[11] M. Gourdelier, J. Swain, C. Arone, A. Mouttou, D. Bracquemond, P. Merida, S. Saffarian, S. Lyonnais, C. Favard, D. Muriaux, Sci. Rep. 12 (1) (2022) 14651,
[12] J.R. Lakowicz, Anal. Biochem. (ISSN: 0003-2697) 324 (2004) 153–169.
[13] I. Gryczynski, J. Malicka, Z. Gryczynski, J.R. Lakowicz, J. Phys. Chem. B (ISSN: 1520-6106) 108 (2004) 12568–12574.
[14] K. Balaa, V. Devauges, Y. Goulam, V. Studer, S. Lévêque-Fort, E. Fort, Live cell imaging with surface plasmon-mediated fluorescence microscopy, 2009.
[15] E. Le Moal, E. Fort, S. Lévêque-Fort, F.P. Cordelières, M.-P. Fontaine-Aupart, C. Ricolleau, Biophys. J. (ISSN: 0006-3495) 92 (2007) 2150–2161.
[16] J.Y. Ye, M. Ishikawa, Opt. Lett. (ISSN: 0146-9592) 33 (2008) 1729.
[17] M. Ballarini, F. Frascella, F. Michelotti, G. Digregorio, P. Rivolo, V. Paeder, V. Musi, F. Giorgis, E. Descrovi, Appl. Phys. Lett. (ISSN: 0003-6951) 99 (2011) 043302.
[18] R. Badugu, K. Nowaczyk, E. Descrovi, J.R. Lakowicz, Anal. Biochem. 442 (1) (2013) 83–96.
[19] A. Angelini, E. Enrico, N.D. Leo, P. Munzert, L. Boarino, F. Michelotti, F. Giorgis, E. Descrovi, New J. Phys. (ISSN: 1367-2630) 15 (2013) 073002.
[20] K. Toma, E. Descrovi, M. Toma, M. Ballarini, P. Mandracci, F. Giorgis, A. Mateescu, U. Jonas, W. Knoll, J. Dostálek, Biosens. Bioelectron. (ISSN: 0956-5663) 43 (2013) 108–114.
[21] E. Descrovi, D. Morrone, A. Angelini, F. Frascella, S. Ricciardi, P. Rivolo, N.D. Leo, L. Boarino, P. Munzert, F. Michelotti, F. Giorgis, Eur. Phys. J. D (ISSN: 1434-6060) 68 (2014).
[22] M.C.D. Santos, R. Déturche, C. Vézy, R. Jaffiol, Opt. Lett. (ISSN: 0146-9592) 39 (2014) 869.
[23] K. Ray, R. Badugu, J.R. Lakowicz, RSC Adv. (ISSN: 2046-2069) 5 (2015) 54403–54411.
[24] F. Michelotti, R. Rizzo, A. Sinibaldi, P. Munzert, C. Wachter, N. Danz, Opt. Lett. (ISSN: 0146-9592) 42 (2017) 2798.
[25] A. Mouttou, F. Lemarchand, C. Koc, A. Moreau, J. Lumeau, C. Favard, A.L. Lereu, Opt. Express 30 (9) (2022) 15365–15375.
[26] A. Sinibaldi, N. Danz, E. Descrovi, P. Munzert, U. Schulz, F. Sonntag, L. Dominici, F. Michelotti, Sensors Actuators B (ISSN: 0925-4005) 174 (2012) 292–298.
[27] S.D. Choudhury, R. Badugu, J.R. Lakowicz, Acc. Chem. Res. (ISSN: 0001-4842) 48 (2015) 2171–2180.
[28] A.L. Lereu, M. Zerrad, A. Passian, C. Amra, Appl. Phys. Lett. (ISSN: 0003-6951) 111 (2017) 011107.
[29] T.G. Mayerhoefer, S. Pahlow, J. Popp, Nanophotonics (ISSN: 2192-8614) 9 (2020) 741–760.
[30] C. Ndiaye, F. Lemarchand, M. Zerrad, D. Ausserré, C. Amra, Appl. Opt. (ISSN: 0003-6935) 50 (2011) C382.
[31] A.L. Lereu, M. Zerrad, M. Petit, F.D. Fornel, C. Amra, SPIE Proc. 9162 (2014) 916219.
[32] A.L. Lereu, M. Zerrad, C. Ndiaye, F. Lemarchand, C. Amra, Appl. Opt. (ISSN: 1559-128X) 53 (2014) A412.
[33] C. Amra, M. Zerrad, F. Lemarchand, A. Lereu, A. Passian, J.A. Zapien, M. Lequime, Phys. Rev. A 97 (2018) 023819.
[34] D. Niu, M. Zerrad, A. Lereu, A. Moreau, J. Lumeau, J.A. Zapien, A. Passian, V. Aubry, C. Amra, Phys. Rev. Appl. 13 (2020) 054064.
[35] M. Zerrad, A.L. Lereu, C. Ndiaye, F. Lemarchand, C. Amra, Opt. Express (ISSN: 1094-4087) 25 (2017) 14883.
[36] A.L. Lereu, F. Lemarchand, M. Zerrad, D. Niu, V. Aubry, A. Passian, C. Amra, Opt. Express (ISSN: 1094-4087) 27 (2019) 30654.